Biosensors and Bioelectronics 178 (2021) 113020

Contents lists available at ScienceDirect

Biosensors and Bioelectronics

journal homepage: http://www.elsevier.com/locate/bios

A microfluidic biosensor for rapid and automatic detection of *Salmonella* using metal-organic framework and Raspberry Pi

Wuzhen Qi [a], Lingyan Zheng [a], Sihan Wang [b], Fengchun Huang [a], Yuanjie Liu [a], Haiyang Jiang [b], Jianhan Lin [a,*]

[a] Key Laboratory of Agricultural Information Acquisition Technology, Ministry of Agriculture and Rural Affairs, China Agricultural University, Beijing, 100083, China
[b] Beijing Advanced Innovation Center for Food Nutrition and Human Health, College of Veterinary Medicine, China Agricultural University, Beijing, 100193, China

ARTICLE INFO

Keywords:
Biosensor
Microfluidic chip
Metal-organic framework
Raspberry pi
Salmonella

ABSTRACT

Rapid screening of pathogenic bacteria contaminated foods is crucial to prevent food poisoning. However, available methods for bacterial detection are still not ready for in-field screening because culture is time-consuming; PCR requires complex DNA extraction and ELISA lacks sensitivity. In this study, a microfluidic biosensor was developed for rapid, sensitive and automatic detection of *Salmonella* using metal-organic framework (MOF) NH_2-MIL-101(Fe) with mimic peroxidase activity to amplify biological signal and Raspberry Pi with self-developed App to analyze color image. First, the target bacteria were separated and concentrated with the immune magnetic nanobeads (MNBs), and labeled with the immune MOFs to form MNB-*Salmonella*-MOF complexes. Then, the complexes were used to catalyze colorless o-phenylenediamine and H_2O_2 to produce yellow 2,3-diaminophenazine (DAP). Finally, the image of the catalysate was collected under the narrow-band blue light and analyzed using the Raspberry Pi App to determine the bacterial concentration. The experimental results showed that this biosensor was able to detect *Salmonella* Typhimurium from 1.5×10^1 to 1.5×10^7 CFU/mL in 1 h with the lower detection limit of 14 CFU/mL. The mean recovery for *Salmonella* in spiked chicken meats was ~112%. This biosensor integrating mixing, separation, labelling and detection onto a single microfluidic chip has demonstrated the merits of automatic operation, fast reaction, less reagent and small size, and is promising for in-field detection of foodborne bacteria.

1. Introduction

Salmonella is one of the main foodborne pathogenic bacteria globally. It has been found in a wide range of foods and resulted in diarrhea, gastroenteritis, typhoid and other symptoms. Rapid and sensitive detection of *Salmonella* is a key measure to prevent and control foodborne diseases (Silva et al., 2018). At present, the common bacterial detection methods mainly include culture, enzyme-linked immunosorbent assay (ELISA) and polymerase chain reaction (PCR) (Kong et al., 2002). However, these methods either are time consuming, or lack sufficient sensitivity, or require complex sample pretreatment. Therefore, it is an urgent demand to develop simple, rapid and sensitive methods to detect *Salmonella*.

In recent years, microfluidics has played an increasing role in the detection of foodborne pathogens, especially for on-site screening (Sayad et al., 2018; Tian et al., 2016), due to its significant strengths, such as less reagent, fast reaction, automatic operation, small size, etc. (Kant et al., 2018). Many efforts have been made on the development of various microfluidic devices for detection of *Salmonella*. So far, various microfabrication techniques, such as photolithography (Yin et al., 2018; Kavand et al., 2019), 3D printing (Aggas et al., 2020; Kramer et al., 2020) and wax printing (Morbioli et al., 2019; Mohammadifar et al., 2018), have been applied to develop microfluidic chips, which could be further combined with immunological assays (Shen et al., 2018; Liu et al., 2018) and molecular biological assays (Srinivasan et al., 2018; Santiago et al., 2018) for *Salmonella* detection. Besides, smartphone is often used with microfluidic chips and fluorescent materials, such as upconversion nanoparticles (Jin et al., 2018), quantum dots (Wang et al., 2020; Tran et al., 2019) and fluorescent microspheres (Wang et al., 2019; Yelleswarapu et al., 2019), to develop portable devices for in-field detection of *Salmonella*. However, these studies are still faced with low sensitivity due to the small sample volume.

Metal-organic frameworks (MOFs), which are formed using organic ligands and metal ions (or clusters) through self-assembly, are a kind of

* Corresponding author.
E-mail address: jianhan@cau.edu.cn (J. Lin).

https://doi.org/10.1016/j.bios.2021.113020
Received 17 December 2020; Accepted 18 January 2021
Available online 21 January 2021

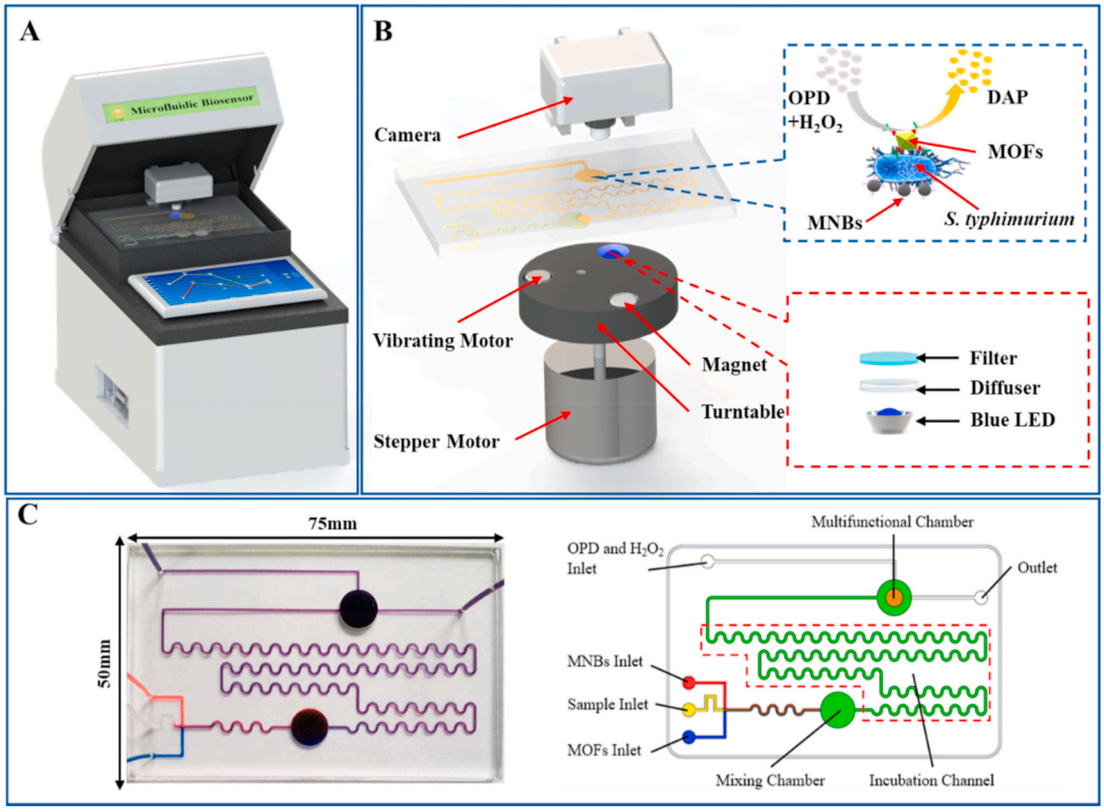

Fig. 1. (A) The prototype of this microfluidic biosensor; (B) The principle and the structure of this microfluidic biosensor; (C) The diagram of the microfluidic chip.

porous crystal materials with high specific surface area and have been frequently reported to enhance the sensitivity of biosensors (Furukawa et al., 2013; Li et al., 2012; Jiao et al., 2019). Some MOFs with unsaturated metallic nodes, such as UIO-66 and MIL-101, were verified with the catalytic properties of biomimetic enzymes and used for amplify biological signals in bacterial detection (Kang et al., 2019; Zhang et al., 2019a; Zhu et al., 2017; Vermoortele et al., 2013; Henschel et al., 2008; Wang et al., 2017). As a peroxidase-like nanozyme, the NH_2-MIL-101 MOFs have been demonstrated to catalyze hydrogen peroxide (H_2O_2) and o-phenylenediamine (OPD) to produce yellow catalysate, 2,3-diaminophenazine (DAP), with an absorption peak at 450 nm (Li et al., 2019). The absorption is often measured by an expensive spectrophotometer, however the sensitivity is generally not high. Thus, it is of great importance to develop simple and sensitive methods for determination of the catalysate when the NH_2-MIL-101 MOFs are employed for amplifying the biological signals to improve the sensitivity of biosensors.

In this study, a microfluidic biosensor was developed for rapid and automatic detection of *Salmonella*. As shown in Fig. 1, the target *Salmonella* cells were simultaneously conjugated with the anti-*Salmonella* monoclonal antibodies modified magnetic nanobeads (MNBs) and the anti-*Salmonella* polyclonal antibodies modified MOFs using an active vibrating mixer and a serpentine incubating channel in a microfluidic chip, resulting in the forming of MNB-*Salmonella*-MOF sandwich complexes. After the complexes were magnetically separated and concentrated in a multifunctional chamber by applying an external magnetic field, the mixture of OPD and H_2O_2 was then injected into the chamber and catalyzed by the MOFs on the complexes to produce DAP. Finally, an image of the catalysate (DAP) was collected under a narrow-band blue light and analyzed using a Raspberry Pi based device with a self-developed App to determine the concentration of the *Salmonella* cells.

2. Materials and methods

2.1. Materials

Salmonella typhimurium (ATCC 14082) was used as target bacteria, *Salmonella* enteritidis, *Listeria monocytogenes* (ATCC 13932) and *E. coli* O157:H7 (ATCC 43888) were used as non-target bacteria. The biotinylated anti-*Salmonella* monoclonal antibodies (mAbs, 2.5 mg/mL) from Meridian (Memphis, TN, USA) and the anti-*Salmonella* polyclonal antibodies (pAbs, 1 mg/mL) from Abcam (Cambridge, MA, USA) were used to specifically react with target *Salmonella* typhimurium. The streptavidin labeling kit from Elabscience (Wuhan, China) was used to modify streptavidin onto the carboxylate magnetic nanobeads (~180 nm, 10 mg/mL) from So-Fe Biomedicine (Shanghai, China). TCO-PEG4-NHS ester (TCO) and tetrazine-sulfo-NHS ester (Tz) from Click Chemistry Tools Bioconjugate (Scottsdale, AZ, USA) were used to conjugate the MOFs with the polyclonal antibodies. Ferric chloride hexahydrate ($FeCl_3{\cdot}6H_2O$) and N, N-dimethylformamide (DMF) from Aladdin (Shanghai, China) and 2-Amino-benzenedicarboxylic acid (NH_2-BDC) from TCI (Shanghai, China) were used to synthesize the NH_2-MIL-101 MOFs. OPD and H_2O_2 from Aladdin were used as the substrate. Phosphate buffered saline from Sigma Aldrich (10 times concentrated, St. Louis, MO, USA) was diluted with deionized water to prepare the PBS solution (pH 7.4, 10 mM). Bovine serum albumin (BSA, 1% and 10%, w/v) from Sigma Aldrich was used for blocking. Tween 20 from Amresco (Solon, OH, USA) was used for washing. The deionized water was produced by Millipore Advantage 10 (18.2 MΩ cm, Billerica, MA, USA) and used for preparing all the solutions.

2.2. Fabrication of the microfluidic chip

This microfluidic biosensor mainly included two parts: a microfluidic chip and a portable device. The microfluidic chip was the key to this biosensor, which integrated mixing, incubation, separation and

detection. As shown in Fig. 1C, this chip mainly consists of three parts: (1) an active vibrating mixer for efficient mixing of the MNBs, the sample and the MOFs, (2) a serpentine incubating channel for sufficient forming of the MNB-*Salmonella*-MOF sandwich complexes, and (3) a multifunctional chamber for magnetic separation of the complexes, MOF catalysis of OPD and H_2O_2, and optical detection of the catalysate. This active mixer was developed using a vibrating motor (TEJIATE-0827, size: φ8mm × 3 mm, TEJIATE, Shenzhen, China) on a turntable to vibrate the circular mixing chamber (size: φ8mm × 3 mm) through a rubber mat, which was filled with the MNBs, the sample and the MOFs. This incubating channel had a width of 600 μm, a height of 600 μm and a total length about of 400 mm, allowing ~5 min's incubation at the flowrate of 30 μL/min. This multifunctional chamber (size: φ8mm × 3 mm) was used with a permanent magnet (size: φ8mm × 3.5 mm, material: NdFeB, grade: N52) on the turntable to magnetically separate the complexes and thoroughly remove the background, and also used for MOF catalysis and optical detection.

This microfluidic chip was fabricated using 3D printing and surface plasma bonding. First, the Object 30 3D printer (material: VeroWhitePlusRGD835, Stratasys, Eden Prairie, MN, USA) was used to print the Resin mold of the microfluidic channel. Then, the mixture of the poly (dimethoxy)silane (PDMS) prepolymer and the curing agent at the ratio of 10:1 from Dow Corning (Sylgard 184, Auburn, MI, USA) was poured into the mold and cured at 60 °C for 8 h. Finally, the cured PDMS channel was removed from the mold and bonded with a thin PDMS membrane with the thickness of 200 μm from Bald Advanced Materials (7101, Hangzhou, China) to obtain the microfluidic chip (size: 50 mm × 75 mm × 5 mm), after their surfaces were treated by plasma.

2.3. Development of the portable device

The portable device (Fig. 1A and Fig. S1) was developed based on Raspberry Pi to control the solutions, rotate the turntable, and analyze the image. As shown in Fig. S2, the solutions were automatically controlled using the self-developed App on the Raspberry Pi (4 B, Raspberry Pi Foundation, Pencoed, UK) through the precise peristaltic pumps (YW01, YW' fluid, Changzhou, China) to achieve the injection, mixing, incubation, washing and reaction. The vibrating motor, the permanent magnet and a blue LED (wavelength: 450 nm) were mounted on the turntable with an interval of 120°, which was also controlled using the App on the Raspberry Pi through a stepper motor (28BYG-48, Risym, Shenzhen, China) and set up under the microfluidic chip. The blue LED, the permanent magnet and the vibrating motor were rotated to the bottom of the mixing chamber and multifunctional chamber by the stepper motor according to the designated protocol, respectively. An enclosure (size: 80 mm × 90 mm × 60 mm) was 3D printed and painted with black matte paint to form an optical darkroom to house the device. The image of the catalysate was collected using the Raspberry Pi camera in the darkroom and analyzed using the self-developed App. The image and result were displayed on the LCD display and transmitted to a self-developed cloud platform through WIFI for data storage and further risk assessment. Besides, an optical diffuser (PMMA, Pengfeng Plastic, Foshan, China) was used with the blue LED to emit the parallel beams with the diameter of 7.5 mm, and a narrow-band filter (wavelength range: 440–460 nm, HS-450ZDLGP, Huashang Laser, Shenzhen, China) was placed between the diffuser and the multifunctional chamber to filter the interference beams. This App was developed in Python environment based on the OpenCV function library using PyCharm IDE with three functions: (1) automatically control the stepper motor to rotate the blue LED, the magnet and the vibrating motor to their designated positions at their designated time, (2) automatically operate the fluids to achieve the mixing, incubation, separation, washing and catalysis, and (3) automatically collect the catalysate image under the blue LED and analyze the image to determine the bacterial concentration. All the procedures for separation, labeling, catalysis and detection were automatically carried out after the "Start" button on the App was activated.

2.4. Preparation of the immune MOFs

The NH_2-MIL-101 MOFs were synthesized according to a previous report (Li et al., 2019). The detailed protocol could be found in the supplemental material. The immune MOFs were synthesized based on the click reaction of Tz and TCO, which were dissolved in 10 mM DMF. First, 4 mg of the MOFs and 200 μg of the pAbs were mixed with TCO and Tz at the molar ratio of 1:40 and incubated for 45 min, respectively. Then, the TCO-MOFs were obtained by centrifuging at 4000×*g* for 10 min, and the Tz-pAbs were obtained by filtering at 10 kDa and centrifuging at 15,000×*g* for 10 min at 4 °C. After the TCO-MOFs and Tz-pAbs were washed with deionized water three times to remove excess labeling reagents and mixed at 15 rpm for 45 min, 1% BSA was used to block the redundant binding sites. Finally, the immune MOFs were obtained after washing with deionized water three times and stored at 4 °C for further use.

2.5. Detection of the target bacteria in pure culture

To detect unknown concentrations of target bacteria, the calibration curve between the absorbance and logarithm of the bacterial concentration was established. Different concentrations of *Salmonella* typhimurium ranging from 1.5×10^1 to 1.5×10^7 CFU/mL were detected using this biosensor. Prior to the test, the immune MNBs were prepared using the biotinylated mAbs and the MNBs, which were modified with streptavidin through EDC/NHS method according to our previous report (Zhang et al., 2019b). The experimental procedure for bacterial detection can be seen in Video S1. As shown in Figs. S3 and 500 μL of the bacterial sample at each concentration (1.5×10^1–1.5×10^7 CFU/mL), 20 μg of the immune MNBs (in 500 μL of deionized water) and 80 μg of the immune MOFs (in 500 μL of deionized water) were simultaneously injected into the microfluidic chip at a flow rate of 30 μL/min, respectively, followed by mixing in the vibrating mixer and incubating in the serpentine channel, resulting in the forming of the MNB-*Salmonella*-MOF complexes. After the complexes were captured in the multifunctional chamber by rotating the permanent magnet under the chamber and washed with deionized water to remove the unbound MOFs, 100 μL of OPD (0.1 M) and 100 μL of H_2O_2 (0.3 mM) were mixed as the substrate and injected into the chamber. Then, as shown in Video S2, the vibrating motor was rotated under the chamber to enhance the catalytic reaction for 15 min to produce the catalysate (DAP). Finally, the blue LED was rotated under the chamber to irradiate the catalysate, and the Raspberry Pi camera on the top of the multifunctional chamber was used to collect the image, which was further analyzed to determinate the bacterial concentration.

2.6. Detection of the target bacteria in spiked chicken meats

To evaluate the practicability of this biosensor, the chicken meats purchased from a local supermarket were spiked with target bacteria and detected using this biosensor. First, 25 g of chicken meats were placed in a sterile plastic bag containing 225 mL of PBS and homogenized by a stomacher (BagMixer CC, InterScience, Paris, France) for 2 min, followed by standing for 5 min to obtain the supernatant. Then, different concentrations of *Salmonella* typhimurium were added into the supernatant to prepare the spiked chicken samples with the bacterial concentration of 1.6×10^1–1.6×10^6 CFU/mL. Finally, the spiked chicken samples were detected using this microfluidic biosensor according to the protocol in Section 2.5.

3. Results and discussion

3.1. Characterization of the NH_2-MIL-101 MOFs

The NH_2-MIL-101 MOFs are the important material for this microfluidic biosensor. Thus, the transmission electron microscopy (TEM), X-

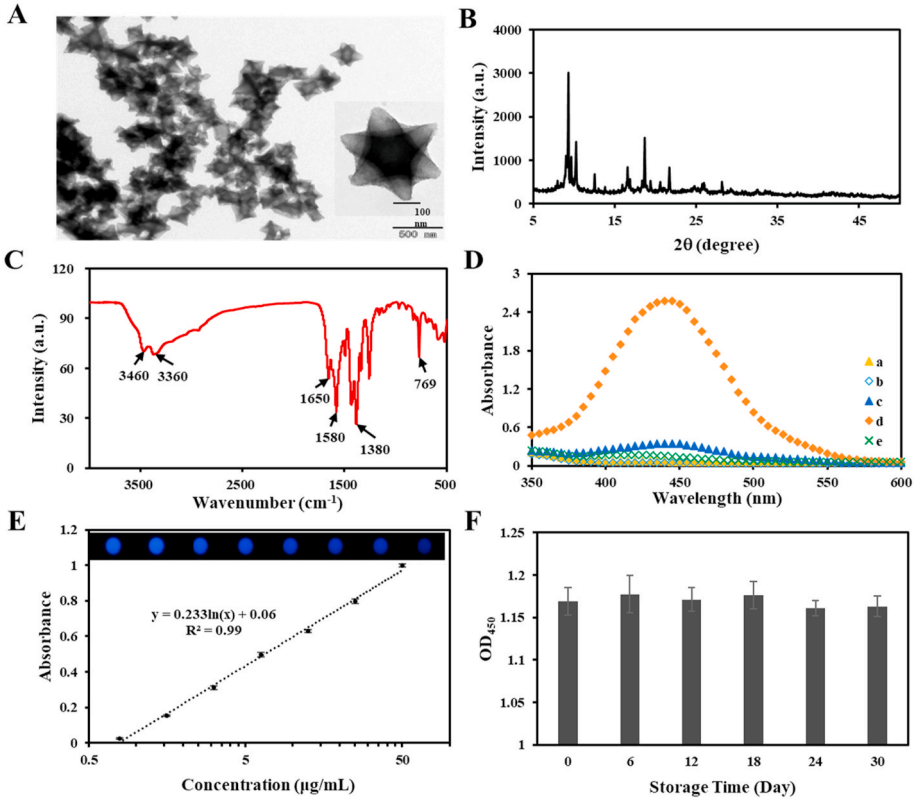

Fig. 2. (A) The TEM image of the MOFs; (B) The XRD profile of the MOFs; (C) The FT-IR spectrum of the MOFs; (D) The absorption spectra for (a) MOFs + OPD, (b) MOFs + H_2O_2, (c) H_2O_2+OPD, (d) MOFs + H_2O_2+OPD and (e) MOFs; (E) The linear relationship between the absorbance and logarithm of the bacterial concentration (N = 3); (F) The stability of the MOFs within 30 days (N = 3).

ray diffraction (XRD) and Fourier transform infrared (FTIR) were used to characterize the MOFs. The TEM images in Fig. 2A show that the NH_2-MIL-101 MOFs have an octahedral structure with a uniform crystal size of ~400 nm. The XRD pattern in Fig. 2B displays that the typical diffraction peaks of the MOFs at 2θ of 9.2, 10.2 and 18.7 (Li et al., 2019), indicating that the MOFs have a complete crystal structure. The FTIR

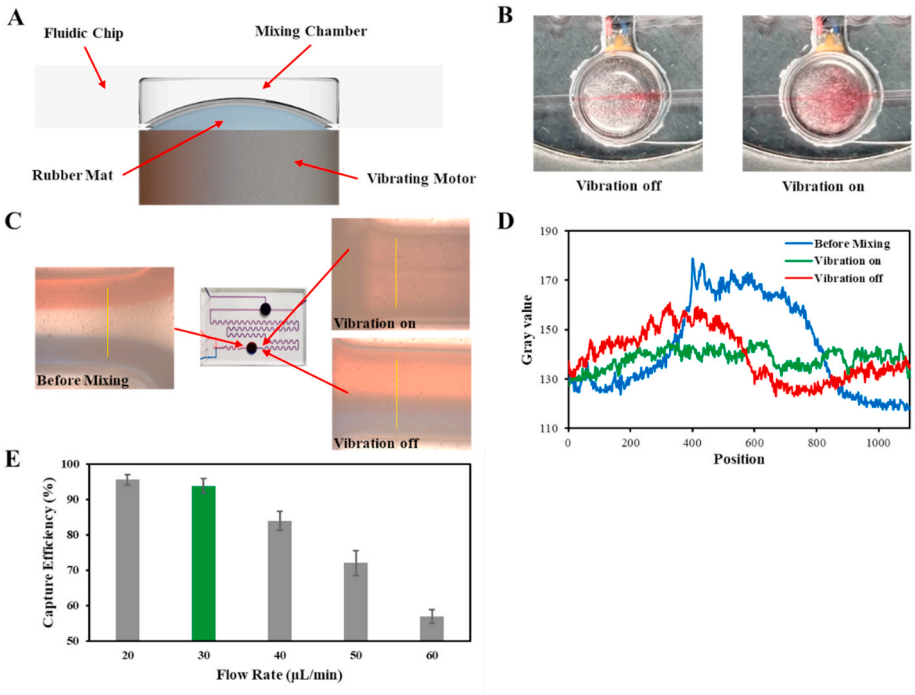

Fig. 3. (A) The structure of this vibrating mixer; (B–C) The evaluation of this vibrating mixer using dye mixing; (D) The gray value analysis of the images; (E) The comparison on the separation efficiency of target bacteria at different flow rates from 20 to 60 μL/min (N = 3).

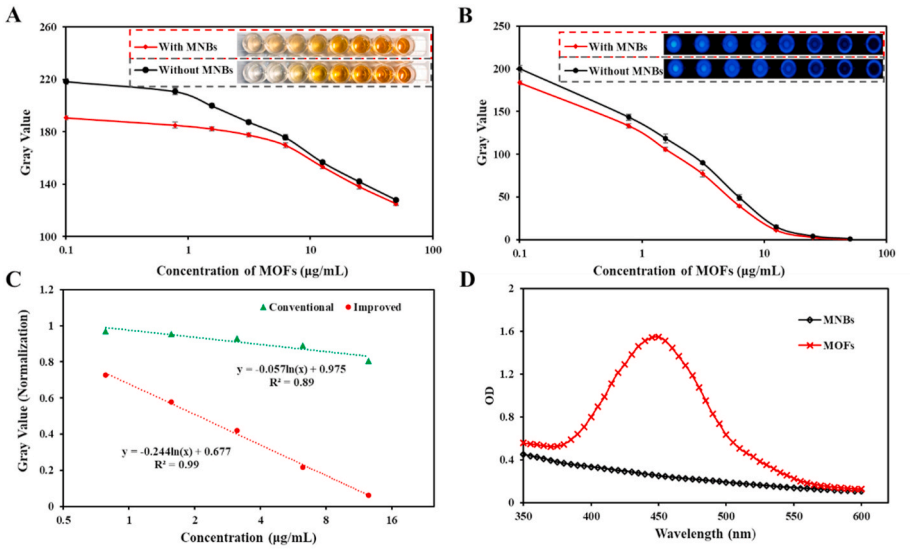

Fig. 4. (A) The gray values of the images with and without the MNBs using the conventional image processing (N = 3); (B) The gray values of the images with and without the MNBs using the improved image processing (N = 3); (C) The comparison of these two image processing methods (N = 3); (D) The absorption spectra for the MNBs and the MOFs (catalysate).

spectrum in Fig. 2C demonstrates that the MOFs have four obvious characteristic absorption peaks at 1650, 1580, 1380 and 769 cm^{-1}, revealing the vibration of the carboxylate groups. The peaks at 3460 and 3360 cm^{-1} are attributed to asymmetrical and symmetrical amine stretching (Li et al., 2016).

Besides, the peroxidase-like characteristic of the NH_2-MIL-101 MOFs was verified. First, 10 μg of the MOFs were added into 500 μL of acetate buffer (pH 4.0). Then, 50 μL of H_2O_2 (3 mM) and/or 50 μL of OPD (0.1 M) were added and incubated at 37 °C for 20 min. Finally, the absorption spectra of different mixtures between 350 nm and 600 nm were recorded. As shown in Fig. 2D, when H_2O_2 or OPD are added into the NH_2-MIL-101 MOFs, no color change is observed in 20 min. However, when H_2O_2 and OPD are added, the color turns yellow rapidly. These results show that the NH_2-MIL-101 MOFs have a good peroxidase-like enzymatic activity. Furthermore, different concentrations (0.78–50 μg/mL) of MOFs were used to react with the substrate and their absorbance was measured using this device. As shown in Fig. 2E, a good linear relationship between the absorbance (***A***) and logarithm of the concentration (***C***) is found and can be described as $\boldsymbol{A} = 0.233 \ln(\boldsymbol{C}) + 0.06$ ($R^2 = 0.99$). To verify their stability, the MOFs were stored at room temperature and used to catalyze the substrate every six days, and the absorbance was detected using the microplate reader. As shown in Fig. 2F, the absorbance for different time almost remain at the same level with a standard deviation of ~2%, indicating that the catalytic activity of the MOFs is stable at room temperature within 30 days.

3.2. Mixing efficiency of the vibrating mixer

The vibrating mixer is a key part of the microfluidic chip, and its mixing efficiency has great impact on the sensitivity of this microfluidic biosensor. To achieve non-contact and efficient mixing, a rubber mat was used as medium to transfer the vibration of the motor into the mixing chamber (Fig. 3A). The mixing effect was evaluated using dye mixing and magnetic separation. The deionized water (top), the red dye (medium) and the deionized water (bottom) were simultaneously injected to the mixer for observation of the mixing effect. As shown in Fig. 3B, when the vibrating mixer is turned off, the central red dye is clearly separated from two sides' water. However, when the mixer is turned on, the red dye and the water are well mixed, which can be observed from Video S3. As shown in Fig. 3C, the red dye (top), the blue dye (bottom) and the deionized water (medium) were simultaneously injected into the mixer and the images at the inlet and outlet of the mixing chamber were taken by an optical microscope (Motic 102 m, Motic, Xiamen, China). To clearly understand the mixing effect, the gray values of the cross section (yellow lines in Fig. 3C) were obtained and shown in Fig. 3D. There are two clear boundary lines at the inlet (Fig. 3C) and the gray values from top to bottom have three obvious levels (Fig. 3D), indicating these three solutions are separate. However, the color looks uniform at the outlet when the vibrating mixer was turned on and the gray values from top to bottom are basically consistent, indicating these solutions are well mixed. When the vibrating mixer is turned off, the medium deionized water disappears because it is mixed with the red and blue dyes from top and bottom sides mainly due to the diffusion, respectively. There still is an obvious boundary line between the red dye and the blue dye and the gray values from top to bottom have two different levels, indicating these solutions are not well mixed.

To further evaluate the mixing efficiency, 1 mL of the bacterial sample at 1.7×10^3 CFU/mL was injected with 20 μg of the immune MNBs into the microfluidic chip at different flow rates from 20 μL/min to 60 μL/min. After incubation in the serpentine channel, the MNP-*Salmonella* complexes were collected and magnetically separated for culture plating. The separation efficiency was calculated as the ratio of the separated bacterial concentration to the original one and used to evaluate the mixing effect. As shown in Fig. 3E, when the flow rate decreases from 60 μL/min to 30 μL/min, the separation efficiency increases from 58.7% to 93.8%. This is because the target *Salmonella* cells have longer time to mix and incubate with the MNBs at lower flow rates, resulting in the forming of more MNB-*Salmonella* complexes. The further decrease on the flow rate to 20 μL/min only results in 1.8% increase on the efficiency, indicating that the flow rate is low enough to allow sufficient reaction between the bacterial cells and the MNBs. Therefore, the flow rate of 30 μL/min was used in this study.

3.3. Processing of the collected images

Since the processing of the catalysate's image is subject to the interferences from the MNBs and the environment, the darkroom and optical filter were employed to minimize the influence. In general, to determine the concentration of the catalysate, its color change is measured using a spectrophotometer to obtain the absorbance, or its color image under the ambient light is collected using a camera and

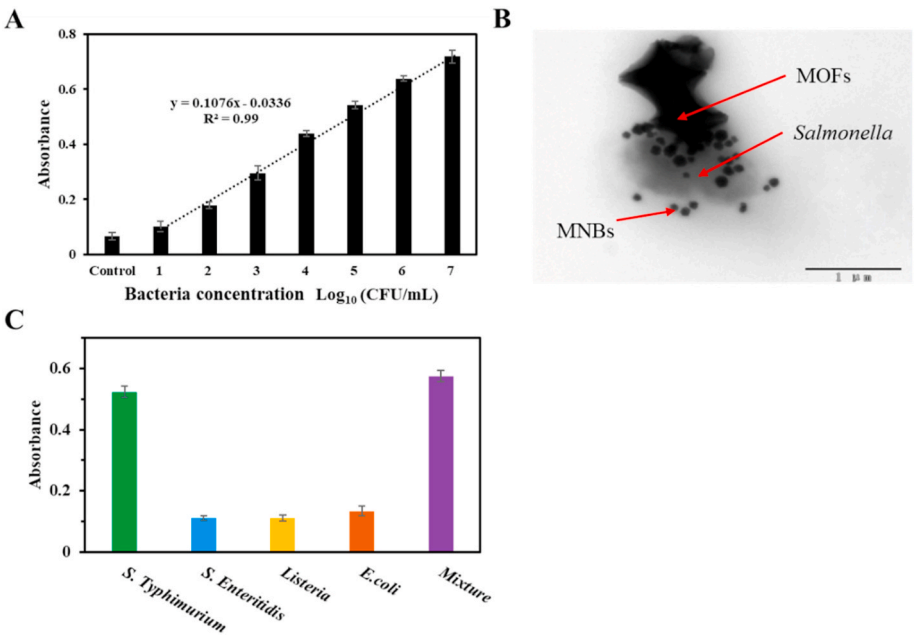

Fig. 5. (A) The calibration curve of this microfluidic biosensor for detection of *Salmonella* Typhimurium (N = 3); (B) The TEM image of the MNB-*Salmonella*-MOF complexes; (C) The specificity of the microfluidic biosensor (N = 3).

processed to obtain the gray, RGB or HSV values (Coleman et al., 2019; Gee et al., 2017; Chen et al., 2019; Nie et al., 2015). However, in this study, it is technically inevitable to suffer the interferences from the MNBs. To understand the influence from the MNBs, 200 μL of the MOFs at different concentrations (0.78–50 μg/mL) were used to catalyze the same volume of the substrate (the mixture of 20 μL of 0.3 mM H_2O_2 and 20 μL of 0.1 M OPD) at the presence and absence of 10 μg MNBs in the 96-well plates, respectively. The images were collected in the darkroom under the visible-band white LED light and the narrow-band blue LED light using this portable device, respectively, and the central area with the size of 20 × 20 pixels was selected from the image for data analysis. For the conventional image processing under the visible-band white light, the selected image was directly grayed to calculate the average gray value. For this improved image processing under the narrow-band blue light, the selected image was first grayed to obtain their average gray value, and then the absorbance (***A***) was calculated, which is defined as.

$\boldsymbol{A} = \lg(\boldsymbol{L_0}/\boldsymbol{L})$Where, $\boldsymbol{L_0}$ and $\boldsymbol{L}$ represent the average gray values for the selected images of deionized water and the catalysate (sample), respectively.

As shown in Fig. 4A, when the conventional image processing is employed, the gray values with the MNBs are lower than those without the MNBs, especially at low concentrations (0.1–1 μg/mL) of the MOFs, because the MNBs absorb partial lights and thus weaken the signal. However, when this improved image processing is employed, the gray value for each image with the MNBs is close to that without the MNBs (Fig. 4B), indicating that the influence from the MNBs has almost been eliminated. To further compare their sensitivity, the images with the MNBs were processed using these two methods. As shown in Fig. 4C, the slope for this improved image processing (0.244) is obviously larger than that for the conventional one (0.057), indicating this improved image processing enhances the sensitivity of this biosensor. This is mainly because only the narrow-band blue light is used to collect the image, resulting in more specific responses to the catalysate (DAP) than the visible-band white light, which can also be verified from Fig. 4D. The MNBs absorb the lights at a wide wavelength range, however the catalysate has a characteristic absorption peak (~1.55) at 450 nm, which is much larger than the MNBs (~0.25). Therefore, when the mixture of the MNBs and the catalysate was irradiated under the 450 nm blue light, the catalysate exhibited a stronger absorption signal, thus reducing the interference of the MNBs.

3.4. Optimization of this microfluidic biosensor

The immune MOFs for labeling the target bacteria and amplifying the detection signal play an important role in the development of this biosensor. Thus, different amounts (20, 40, 60, 80 and 100 μg) of the immune MOFs were used to react with 1 mL of the *Salmonella* cells (1.4×10^5 CFU/mL), respectively. As shown in Fig. S4A, the absorbance increases from 0.09 to 0.49, when the amount of the immune MOFs changes from 20 μg to 80 μg. However, the further increase to 100 μg does not result in an obvious increase, because sufficient MOFs have been used to react with the target bacteria. Thus, the optimal amount of 80 μg for the immune MOFs was used in this study.

The catalytic reaction time also has great impact on the sensitivity of this biosensor. Therefore, different catalytic reaction time from 0 to 20 min was used to detect the target bacteria at the concentration of 1.5×10^5 CFU/mL. The images were collected every 5 min and the absorbance of each image was calculated. As shown in Fig. S4B, the absorbance increases rapidly from 0.126 to 0.502 because more DAP is produced, when the catalytic reaction time changes from 0 to 15 min. However, the further increase to 20 min does not result in an obvious increase on the absorbance. Therefore, the optimal time of 15 min was used in this study.

3.5. Performance evaluation of this microfluidic biosensor

Under the optimal conditions, different concentrations of *Salmonella* Typhimurium ranging from 1.5×10^1 to 1.5×10^7 CFU/mL were detected to obtain the calibration curve using this biosensor. As shown in Fig. 5A, the absorbance increases with the bacterial concentration from 1.5×10^1 to 1.5×10^7 CFU/mL, and a good linear relationship between the absorbance (***A***) and logarithm of the bacterial concentration (***C***) was found and could be expressed as: $\boldsymbol{A} = 0.1076 \log_{10}(\boldsymbol{C}) - 0.0336$ ($R^2 = 0.99$). The low detection limit of this biosensor was determined to be 14 CFU/mL based on 3 times of signal-to-noise ratio. Compared to some recently reported methods for *Salmonella* detection in Table S1, this biosensor has shown a higher or comparable sensitivity, a

Table 1
Detection of *Salmonella* Typhimurium in spiked chicken samples (N = 3).

Added (CFU/mL)	Detected (CFU/mL)	Recovery (%)	CV (%)
16	19	118.75	17.05
160	179	111.88	6.91
1600	1719	107.44	5.4
16000	17531	109.57	6.22
160000	181870	113.67	4.62

higher automatic level, and a shorter detection time. The high sensitivity may be attributed to the following aspects: (1) the high stability (repeatability) of this biosensor due to the fully automatic operations; (2) the efficient reaction of the MNBs and MOFs with the target bacteria due to the active vibrating mixer; (3) the accurate measurement of the image due to the improved image processing under the narrow-band blue light. Besides, TEM was conducted to verify the forming of the MNB-*Salmonella*-MOF sandwich complexes (Fig. 5B).

The specificity of this microfluidic biosensor was evaluated by detecting the target bacteria (*Salmonella* Typhimurium), the non-target bacteria (*Listeria monocytogenes*, *E. coli* O157: H7 and *Salmonella* Enteritidis), and their mixture at the concentration of 10^5 CFU/mL. As shown in Fig. 5C, the absorbance of the non-target bacteria (0.104 for *Listeria monocytogenes*, 0.126 for *E. coli* O157: H7, 0.103 for *Salmonella* Enteritidis) are much lower than those of *Salmonella* Typhimurium (0.502) and their mixture (0.539), indicating that the microfluidic biosensor has a good specificity.

To further demonstrate the practicability of this microfluidic biosensor for detection of *Salmonella* typhimurium in real food samples, three parallel tests on spiked chicken meats (1.6×10^1 to 1.6×10^5 CFU/mL for supernatant or 1.6×10^0 to 1.6×10^4 CFU/g for meat) were conducted using this microfluidic biosensor. The recovery was defined as the ratio of the detected concentration to the added one. As shown in Table 1, the recoveries for different concentrations of spiked samples range from 107.44% to 118.75% with the standard deviations from 4.62% to 17.05%, and the average recovery was 112.26%, indicating this microfluidic biosensor has a good applicability for detection of *Salmonella* Typhimurium in chicken meats. The detected concentrations are a little higher than the added ones mainly due to non-specific adsorption of the MOFs by fats and proteins in chicken samples.

4. Conclusions

In this study, a microfluidic biosensor was successfully developed for rapid, sensitive and automatic detection of *Salmonella* typhimurium. The vibrating mixer was demonstrated to be effective to rapidly mix the solutions and the improved image processing was verified with higher sensitivity. The microfluidic biosensor had successfully integrated mixing, incubation, separation, catalysis and detection, and was able to detect *Salmonella* typhimurium as low as 14 CFU/mL in 1 h. It is worth mentioning that the total cost for this microfluidic biosensor does not exceed US $200, and all the components listed in Table S2 are commercially available. It has the potential to be extended for in-field screening of other foodborne bacteria to ensure food safety.

Declaration of competing interest

The authors declare that they have no known competing financial interests or personal relationships that could have appeared to influence the work reported in this paper.

Acknowledgments

This study was supported in part by the National Natural Science Foundation of China (32071899) and the Walmart Foundation (SA17031161).

Appendix A. Supplementary data

Supplementary data to this article can be found online at https://doi.org/10.1016/j.bios.2021.113020.

References

Aggas, J.R., Abasi, S., Phipps, J.F., Podstawczyk, D.A., Guiseppi-Elie, A., 2020. Microfabricated and 3-D printed electroconductive hydrogels of PEDOT:PSS and their application in bioelectronics. Biosens. Bioelectron. 168, 112568.
Chen, G., Fang, C., Chai, H.H., Zhou, Y., Yun Li, W., Yu, L., 2019. Improved analytical performance of smartphone-based colorimetric analysis by using a power-free imaging box. Sensor. Actuator. B Chem. 281, 253–261.
Coleman, B., Coarsey, C., Kabir, M.A., Asghar, W., 2019. Point-of-care colorimetric analysis through smartphone video. Sensor. Actuator. B Chem. 282, 225–231.
Furukawa, H., Cordova, K.E., O'Keeffe, M., Yaghi, O.M., 2013. The chemistry and applications of metal-organic frameworks. Science 341 (6149), 1230444.
Gee, C.T., Kehoe, E., Pomerantz, W.C.K., Penn, R.L., 2017. Quantifying protein concentrations using smartphone colorimetry: a new method for an established test. J. Chem. Educ. 94 (7), 941–945.
Henschel, A., Gedrich, K., Kraehnert, R., Kaskel, S., 2008. Catalytic properties of MIL-101. Chem. Commun. 35, 4192–4194.
Jiao, L., Seow, J.Y.R., Skinner, W.S., Wang, Z.U., Jiang, H.-L., 2019. Metal–organic frameworks: structures and functional applications. Mater. Today 27, 43–68.
Jin, B., Yang, Y., He, R., Park, Y.I., Lee, A., Bai, D., Li, F., Lu, T.J., Xu, F., Lin, M., 2018. Lateral flow aptamer assay integrated smartphone-based portable device for simultaneous detection of multiple targets using upconversion nanoparticles. Sensor. Actuator. B Chem. 276, 48–56.
Kang, Y.-S., Lu, Y., Chen, K., Zhao, Y., Wang, P., Sun, W.-Y., 2019. Metal–organic frameworks with catalytic centers: from synthesis to catalytic application. Coord. Chem. Rev. 378, 262–280.
Kant, K., Shahbazi, M.-A., Dave, V.P., Ngo, T.A., Chidambara, V.A., Than, L.Q., Bang, D. D., Wolff, A., 2018. Microfluidic devices for sample preparation and rapid detection of foodborne pathogens. Biotechnol. Adv. 36 (4), 1003–1024.
Kavand, H., van Lintel, H., Bakhshi Sichani, S., Bonakdar, S., Kavand, H., Koohsorkhi, J., Renaud, P., 2019. Cell-imprint surface modification by contact photolithography-based approaches: direct-cell photolithography and optical soft lithography using PDMS cell imprints. ACS Appl. Mater. Interfaces 11 (11), 10559–10566.
Kong, R.Y.C., Lee, S.K.Y., Law, T.W.F., Law, S.H.W., Wu, R.S.S., 2002. Rapid detection of six types of bacterial pathogens in marine waters by multiplex PCR. Water Res. 36 (11), 2802–2812.
Kramer, R., Verlinden, E.J., Angeloni, L., van den Heuvel, A., Fratila-Apachitei, L.E., van der Maarel, S.M., Ghatkesar, M.K., 2020. Multiscale 3D-printing of microfluidic AFM cantilevers. Lab Chip 20 (2), 311–319.
Li, J.R., Sculley, J., Zhou, H.C., 2012. Metal-organic frameworks for separations. Chem. Rev. 112 (2), 869–932.
Li, X., Pi, Y., Xia, Q., Li, Z., Xiao, J., 2016. TiO2 encapsulated in Salicylaldehyde-NH2-MIL-101(Cr) for enhanced visible light-driven photodegradation of MB. Appl. Catal. B Environ. 191, 192–201.
Li, S., Hu, X., Chen, Q., Zhang, X., Chai, H., Huang, Y., 2019. Introducing bifunctional metal-organic frameworks to the construction of a novel ratiometric fluorescence sensor for screening acid phosphatase activity. Biosens. Bioelectron. 137, 133–139.
Liu, C., Xu, X., Li, B., Situ, B., Pan, W., Hu, Y., An, T., Yao, S., Zheng, L., 2018. Single-exosome-counting immunoassays for cancer diagnostics. Nano Lett. 18 (7), 4226–4232.
Mohammadifar, M., Zhang, J., Yazgan, I., Sadik, O., Choi, S., 2018. Power-on-paper: origami-inspired fabrication of 3-D microbial fuel cells. Renew. Energy 118, 695–700.
Morbioli, G.G., Speller, N.C., Cato, M.E., Cantrell, T.P., Stockton, A.M., 2019. Rapid and low-cost development of microfluidic devices using wax printing and microwave treatment. Sensor. Actuator. B Chem. 284, 650–656.
Nie, H., Wang, W., Li, W., Nie, Z., Yao, S., 2015. A colorimetric and smartphone readable method for uracil-DNA glycosylase detection based on the target-triggered formation of G-quadruplex. Analyst 140 (8), 2771–2777.
Santiago, P., Jimenez-Belenguer, A., Garcia-Hernandez, J., Estelles, R.M., Hernandez Perez, M., Castillo Lopez, M.A., Ferrus, M.A., Moreno, Y., 2018. High prevalence of Salmonella spp. in wastewater reused for irrigation assessed by molecular methods. Int. J. Hyg Environ. Health 221 (1), 95–101.
Sayad, A., Ibrahim, F., Mukim Uddin, S., Cho, J., Madou, M., Thong, K.L., 2018. A microdevice for rapid, monoplex and colorimetric detection of foodborne pathogens using a centrifugal microfluidic platform. Biosens. Bioelectron. 100, 96–104.
Shen, H., Qu, F., Xia, Y., Jiang, X., 2018. Straightforward and ultrastable surface modification of microfluidic chips with norepinephrine bitartrate improves performance in immunoassays. Anal. Chem. 90 (6), 3697–3702.
Silva, N.F.D., Magalhaes, J., Freire, C., Delerue-Matos, C., 2018. Electrochemical biosensors for Salmonella: state of the art and challenges in food safety assessment. Biosens. Bioelectron. 99, 667–682.
Srinivasan, S., Ranganathan, V., DeRosa, M.C., Murari, B.M., 2018. Label-free aptasensors based on fluorescent screening assays for the detection of Salmonella typhimurium. Anal. Biochem. 559, 17–23.
Tian, F., Lyu, J., Shi, J., Tan, F., Yang, M., 2016. A polymeric microfluidic device integrated with nanoporous alumina membranes for simultaneous detection of multiple foodborne pathogens. Sensor. Actuator. B Chem. 225, 312–318.

Tran, M.V., Susumu, K., Medintz, I.L., Algar, W.R., 2019. Supraparticle assemblies of magnetic nanoparticles and quantum dots for selective cell isolation and counting on a smartphone-based imaging platform. Anal. Chem. 91 (18), 11963–11971.

Vermoortele, F., Bueken, B., Le Bars, G., Van de Voorde, B., Vandichel, M., Houthoofd, K., Vimont, A., Daturi, M., Waroquier, M., Van Speybroeck, V., Kirschhock, C., De Vos, D.E., 2013. Synthesis modulation as a tool to increase the catalytic activity of metal-organic frameworks: the unique case of UiO-66(Zr). J. Am. Chem. Soc. 135 (31), 11465–11468.

Wang, S., Deng, W., Yang, L., Tan, Y., Xie, Q., Yao, S., 2017. Copper-based metal-organic framework nanoparticles with peroxidase-like activity for sensitive colorimetric detection of Staphylococcus aureus. ACS Appl. Mater. Interfaces 9 (29), 24440–24445.

Wang, S., Zheng, L., Cai, G., Liu, N., Liao, M., Li, Y., Zhang, X., Lin, J., 2019. A microfluidic biosensor for online and sensitive detection of Salmonella typhimurium using fluorescence labeling and smartphone video processing. Biosens. Bioelectron. 140, 111333.

Wang, X., Kong, L., Gan, Y., Liang, T., Zhou, S., Sun, J., Wan, H., Wang, P., 2020. Microfluidic-based fluorescent electronic eye with CdTe/CdS core-shell quantum dots for trace detection of cadmium ions. Anal. Chim. Acta 1131, 126–135.

Yelleswarapu, V., Buser, J.R., Haber, M., Baron, J., Inapuri, E., Issadore, D., 2019. Mobile platform for rapid sub-picogram-per-milliliter, multiplexed, digital droplet detection of proteins. Proc. Natl. Acad. Sci. U. S. A. 116 (10), 4489–4495.

Yin, M.J., Zhao, Q., Wu, J., Seefeldt, K., Yuan, J., 2018. Precise micropatterning of a porous poly(ionic liquid) via maskless photolithography for high-performance nonenzymatic H2O2 sensing. ACS Nano 12 (12), 12551–12557.

Zhang, C.-L., Lu, B.-R., Cao, F.-H., Wu, Z.-Y., Zhang, W., Cong, H.-P., Yu, S.-H., 2019a. Electrospun metal-organic framework nanoparticle fibers and their derived electrocatalysts for oxygen reduction reaction. Nanomater. Energy 55, 226–233.

Zhang, H., Xue, L., Huang, F., Wang, S., Wang, L., Liu, N., Lin, J., 2019b. A capillary biosensor for rapid detection of Salmonella using Fe-nanocluster amplification and smart phone imaging. Biosens. Bioelectron. 127, 142–149.

Zhu, L., Liu, X.Q., Jiang, H.L., Sun, L.B., 2017. Metal-organic frameworks for heterogeneous basic catalysis. Chem. Rev. 117 (12), 8129–8176.